PCCP

PAPER

View Article Online
View Journal | View Issue

Cite this: *Phys. Chem. Chem. Phys.*, 2014, **16**, 26273

Achieving a direct band gap in oxygen functionalized-monolayer scandium carbide by applying an electric field†

Youngbin Lee, Yubin Hwang, Sung Beom Cho and Yong-Chae Chung*

Received 25th August 2014,
Accepted 27th October 2014

DOI: 10.1039/c4cp03811h

www.rsc.org/pccp

In the present paper, the band gap characteristics of oxygen functionalized-monolayer scandium carbide (monolayer Sc_2CO_2) under a perpendicular external electric field (E-field) were studied using DFT calculations for the potential application of MXene in optoelectronic and optical nanodevices. In contrast to general pristine single-layer materials under an external E-field, monolayer Sc_2CO_2 undergoes an indirect to direct band gap transition under a positive E-field, and the band gap value changes sharply after the band gap transition. Remarkable variations of the band gap properties are induced by the distinct sensitivity between the Γ and K points in the lowest conduction band to the perpendicular E-field, and different types of orbital lead to the dissimilar response of each point. The present work clearly suggests an effective direction to obtain attractive band gap properties in monolayer MXene using an external E-field for next generation optoelectronic and optical devices.

Introduction

Band gap engineering is an important technology for the design of new materials and devices for semiconducting, optoelectronic, and optical applications.[1,2] In particular, tuning an electronic structure to achieve a direct band gap is essential in fields like optoelectronics and optics. For this reason, previous studies have attempted numerous approaches such as applying a strain or an electric field (E-field), changing the stacking number, and chemical modification to modulate an indirect to direct band gap transition.[2–10] Such diverse endeavors have been conducted in two-dimensional materials such as transition-metal dichalcogenide and GaN nanosheets as well as bulk structures.[2–8]

Recently, among two-dimensional materials, monolayer transition-metal carbides such as Ti_2C, Ti_3C_2, V_2C, Nb_2C, and Ta_4C_3 have been successfully synthesized from MAX phases (M = early transition metal, A = group IIIA or IVA element, X = carbon or nitrogen).[11–14] These new single-layer materials are called MXenes, and they are fabricated through selective etching of the A layers in the MAX phases and sonication.[15,16] From the real etching process, functional groups like F, OH, and O are spontaneously bound to both sides of bare MXene from the etchant, and a terminated MXene is formed.[16] A terminated MXene generally has metallic characteristics, but six types of MXenes, Ti_2CO_2, Zr_2CO_2, Hf_2CO_2, Sc_2CO_2, $Sc_2C(OH)_2$, and Sc_2CF_2, are known to have a semiconducting band gap.[16–18] Among these six semiconducting MXenes, five terminated MXenes except for $Sc_2C(OH)_2$ have an indirect band gap that disturbs efficient light emission, and $Sc_2C(OH)_2$ has a relatively small direct band gap, which corresponds to a long wavelength light emission.[17] Therefore, as earlier attempted in diverse materials, it is necessary to induce an indirect to direct band gap transition in a new two-dimensional material for optoelectronics and optics.

Among the various methods, an external E-field has been commonly applied to many layered structures for modifying their electronic structure because an E-field can be precisely controlled.[3,19–24] Generally, band gap tuning by an external E-field has been used in multilayer systems such as bilayer graphene or transition-metal dichalcogenide, and a multilayer BN-graphene heterostructure.[19–24] This is because in pristine monolayer materials like graphene, silicene, germanene, and GaN under an E-field, the band gap size is little influenced and the band gap transition is not introduced.[24–27] However, a previous study reported that an external E-field leads to a considerable change in the band gap character of the chemically modulated single-layer GaN.[3] From this investigation, it is supposed that other functionalized-monolayers can also be affected by an external E-field.

In the present work, using first-principles density-functional theory (DFT) calculations, an indirect to direct band gap transition in monolayer Sc_2CO_2 was examined by applying a perpendicular external E-field. With the development in synthesis of MXene in the near future, monolayer Sc_2C can be experimentally formed

Department of Materials Science and Engineering, Hanyang University, Seoul, 133-791, Republic of Korea. E-mail: yongchae@hanyang.ac.kr; Tel: +82-2-2220-0507

† Electronic supplementary information (ESI) available. See DOI: 10.1039/c4cp03811h

from bulk Sc_2AC (A = Al, Ga, In, Tl) among the MAX phases.[28] Also, monolayer Sc_2C will be able to undergo spontaneous chemical modulation by the oxygen functional in a real process due to the large negative formation energy.[17] Here, this monolayer Sc_2CO_2 was considered because a previous paper reported that it has the largest band gap among the six semiconducting MXenes mentioned above.[17]

Monolayer MXene has been studied in various fields such as electrochemical energy storage materials and a hydrogen storage medium.[29–38] With such applications, this valuable exploration using monolayer MXene will make the choice more extensive for the design of promising nanodevices in optoelectronics and optics out of pre-existing materials.

Calculation method

The Vienna Ab-initio Simulation Package (VASP) code[39–41] was used for the DFT calculations, and all the calculations were implemented under the Perdew–Burke–Ernzerhof (PBE)[42] generalized gradient approximation (GGA) with a projector augmented wave (PAW) pseudopotential method[43] for the exchange–correlation potential. The plane wave basis was set with a cutoff energy of 500 eV, and a $12 \times 12 \times 1$ Gamma centered Monkhorst–Pack[44] *k*-point grid was used for the Brillouin zone integrations. The atomic positions were optimized using the conjugate gradient method until all the Hellmann–Feynman forces on any atom became less than 0.02 eV $Å^{-1}$. The criterion for energy convergence was 10^{-6} eV per cell, and a Methfessel–Paxton smearing scheme was used with a width of 0.1 eV. The density of states was calculated using a $48 \times 48 \times 1$ Gamma centered Monkhost-Pack *k*-point mesh.

Although MXene exfoliation has not been completely comprehended yet, to model a freestanding monolayer Sc_2CO_2 system, a vacuum spacing of 25 Å was used to avoid any unnecessary interlayer reaction. Monolayer Sc_2C is comprised of a close-packed C layer sandwiched between two close-packed Sc layers, as shown in Fig. S1 (ESI†). It has been discovered that on both sides of the single-layer Sc_2C, two terminated O layers can be positioned with four types (see ESI†).[16] The unit cells of each model were precisely determined by an energy-convergence test. The most stable unit cells turned out to have lattice parameters of 3.24, 3.38, 3.44, and 3.50 Å at Model 1, 2, 3, and 4, respectively (Fig. S1, ESI†).

The calculations of the external E-field on each system were conducted by adding an artificial dipole to the vacuum level.[45] The external E-field was applied perpendicularly to the monolayer Sc_2CO_2 sheet with a range from -5 to 5 V nm^{-1}. Here, a positive value is defined where the external E-field heads from the O_B side to the O_A side in the monolayer Sc_2CO_2 system, and a negative one is in the opposite direction of the positive one (Fig. 1). In the present work, the spin–orbit coupling effect was not considered because the contribution to the band gap transition was negligible.

Results and discussion

Among the four types of monolayer Sc_2CO_2 mentioned above, Model 3 is the most stable structure after chemical modulation

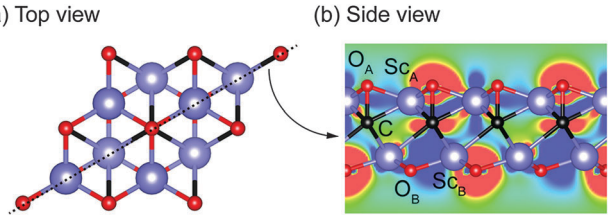

Fig. 1 The most stable configuration of monolayer Sc_2CO_2: (a) top view and (b) side view, respectively. The background of the side view is the charge redistribution at the sliced plane according to the dashed line in the top view when monolayer Sc_2C is functionalized by the O atoms. The red and blue regions represent an accumulation and depletion of electrons, respectively. The isovalues are ±0.005 a.u.

by the O atom. It was still the most stable under a perpendicular external E-field from -5 to 5 V nm^{-1} (Fig. S2, ESI†). From previous work, it has been already determined that the most stable monolayer Sc_2CO_2 has an asymmetric structure, although the same O atoms are terminated on both sides of the monolayer Sc_2C.[17] In the asymmetric structure, the distance between the Sc_A and C atoms (2.21 Å) is closer than that between the Sc_B and C atoms (2.53 Å) because the C atom is bound to the O_A atom (Fig. 1). Since the negatively charged C layer is off-centered along the $+z$-axis by the C–O_A bond, a density of electrons becomes denser in the upper monolayer Sc_2CO_2, as shown in Fig. 1. In addition, it was also observed that a charge depletion region is spread more in the lower monolayer Sc_2CO_2 (Fig. 1). The charge redistribution by asymmetric atomic position induces spontaneous polarization in the monolayer Sc_2CO_2 system, and the polarization leads to an internal E-field in the same direction as the positive external E-field. The phenomenon is verified by the asymmetric electrostatic potential along the *z*-axis and the existence of a dipole in the vacuum level under no external E-field (Fig. S3, ESI†). Consequently, similar to chemically modified GaN by two different atoms,[3] it can be anticipated that the band gap properties of monolayer Sc_2CO_2 respond differently to the direction of the external E-field because of the spontaneous polarization by the asymmetric configuration.

To confirm a response of the band gap of the monolayer Sc_2CO_2 to the external E-field, the band structures under each E-field were examined as shown in Fig. 2. Similar to the band structures of other pristine monolayer systems such as GaN and silicene,[24–27] in the monolayer Sc_2CO_2 system, the configuration of the band structure is maintained under an external E-field. In addition, the original band gap, which is the *K* (conduction band minimum, CBM) to *Γ* (valence band maximum, VBM) indirect band gap of 1.830 eV, is also little affected under a negative and small positive E-field. From the primary band gap, while the band gap size is reduced by 63 meV as the negative external E-field increases to -5 V nm^{-1}, the band gap size is broadened by 39 meV under a positive external E-field of 3 V nm^{-1}. Although the band gap obtained by the opposite external E-field shows dissimilar response as expected in the previous paragraph, a range of the band gap change is too small to manipulate the optical characteristics. However, interestingly,

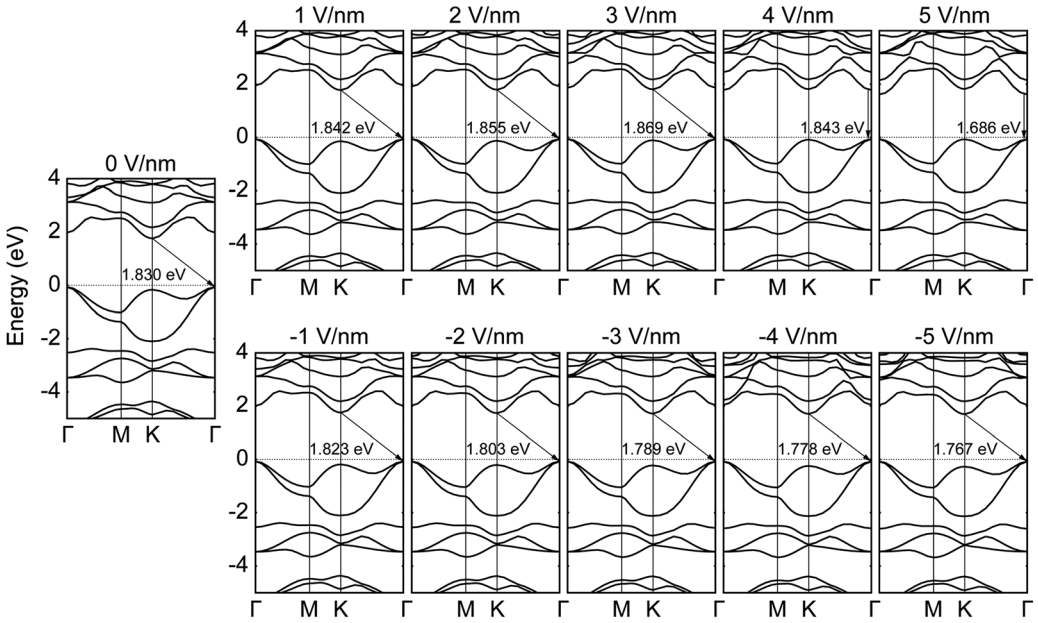

Fig. 2 Band structure in monolayer Sc_2CO_2 under each perpendicular external E-field. The Fermi level was set to zero and the arrows represent the recombination pathways of the excited electron–hole pairs.

the K to Γ indirect band gap is changed to a Γ to Γ direct band gap in the range between 3 and 4 V nm^{-1}. After the indirect to direct band gap transition, the band gap size rapidly decreased by 183 meV during the increment of the positive external E-field by only 2 V nm^{-1}. It is noticeable that the remarkable variation in monolayer Sc_2CO_2 under the external E-field is in stark contrast to results of the general pristine monolayer materials.[24–27]

To analyze the unique changes of the band gap characters in monolayer Sc_2CO_2, variations of the energy gaps between the K and Γ points of the lowest conduction band and the topmost valence band by the external E-field are presented in Fig. 3. The energy gaps are important because the band gap characteristics of monolayer Sc_2CO_2 are decided by the relative location of each point in the lowest condition band and the topmost valence band. Fig. 3(a) shows that the critical point of the indirect to direct band gap transition occurs at about 3.7 V nm^{-1}. With the critical point as the center, the band gap properties undergo drastic variations in their size and direction. As the primary factor of the band gap changes by a perpendicular E-field, it is confirmed that the energy difference between the K and Γ points in the lowest conduction band varies more sensitively with the external E-field than that in the topmost valence band (Fig. 3(b)). Furthermore, by comparing the black (green) line with the blue (red) one in Fig. 3(a), it can be seen that, in the

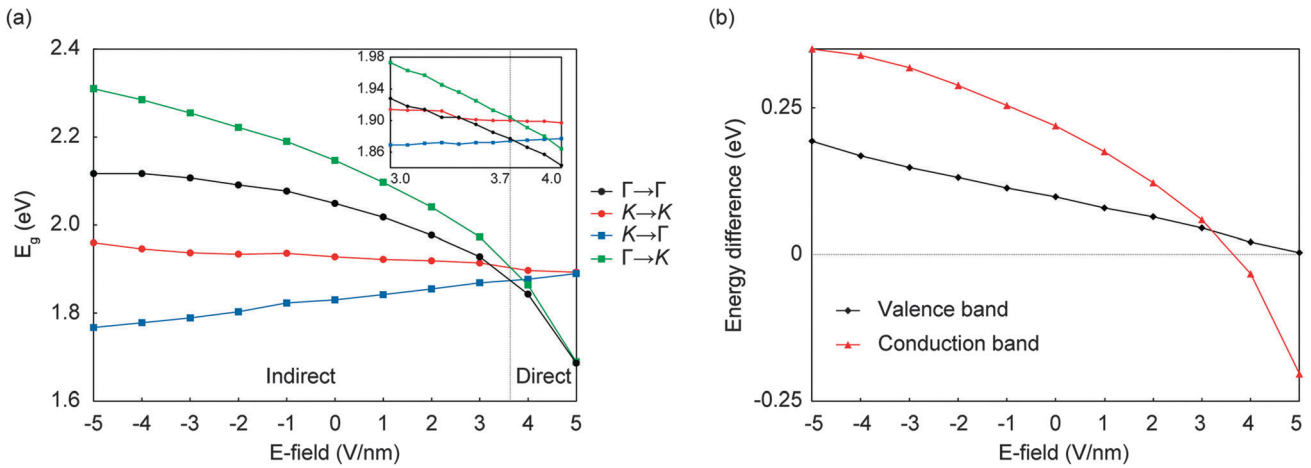

Fig. 3 Change of energy gap between each point in the lowest conduction band and the topmost valence band as a function of the external E-field. (a) Change in the energy gaps from the lowest conduction band to the topmost valence band as a function of the E-field. The black, red, blue, and green lines represent the Γ to Γ, K to K, K to Γ, and Γ to K gap, respectively. (b) Change in the energy difference between the Γ and K point in each lowest conduction band and the topmost valence band as a function of the E-field. The black and red lines represent the variation in the valence band and conduction band, respectively.

lowest conduction band, the energy gap including the Γ point is more susceptible to a perpendicular external E-field than that including the K point. These results indicate that the indirect to direct band gap transition is introduced by a distinction of the responses of each point in the lowest conduction band to the perpendicular E-field. Also, the aspect of variation in the band gap size is explained by the same reason. While the band gap exhibits a linear dependence with a small slope on the intensity of the E-field when the CBM state is the K point, the band gap is changed sharply after the band gap transition when the CBM state turns into the Γ point.

To clarify why the K and Γ points in the lowest conduction band are differently influenced by the perpendicular external E-field, the contributions of atoms to each point were investigated. The contributions of atoms to each energy level are altered by the external E-field only negligibly, as shown in Fig. 4. However, as mentioned above, the point of the CBM state is changed as the energy level is shifted by the external E-field, and as a result, the types of atom composing it are also varied. In the zero field state, the CBM state, which is the K point, mainly originates from the Sc_A atom as 88%. On the other hand, as the external E-field increases to 5 V nm^{-1}, the Sc_A, C, and O_A atoms become the dominant factors of the CBM state at the Γ point and contribute to this state as 24, 30, and 24%, respectively.

To further understand how each atom reacts to the perpendicular external E-field, the partial density of states (PDOS) of the major components are shown in Fig. 5. In the E-field-free state, the d_{xy} and $d_{x^2-y^2}$ orbitals, the so-called in-plane orbitals, of the Sc_A atom primarily have an effect on the CBM state. On the other hand, the CBM state under the perpendicular E-field of 5 V nm^{-1} is mainly contributed by the p_z (out-of-plane) orbital of the C atom and the s orbital of the Sc_A and O_A atoms. The oriented orbitals in the CBM state under 0 and 5 V nm^{-1} can be confirmed in the insets of Fig. 5(a) and (b-ii). In fact, in the lowest conduction band under the external E-field of 0 and 5 V nm^{-1}, 92% of the K point is comprised of the in-plane orbitals (p_x, p_y, d_{xy}, $d_{x^2-y^2}$) in all atoms, and the out-of-plane orbitals (p_z, d_{xz}, d_{yz}, d_{z^2}) of all the components entirely occupy the Γ point except for the non-orientable s orbital. Thus, it can be concluded that in monolayer Sc_2CO_2, the indirect to direct band gap transition and the drastic variation in the band gap size are induced due to the out-of-plane orbitals of the Γ point in the lowest conduction band which are more sensitive to the perpendicular external E-field than the in-plane orbitals of the K point.

Generally, it is well-known that the exact band gap cannot be obtained from regular DFT calculations and the value is underestimated.[46–48] Also, an optical gap, which is correlated with a wavelength of light for applications, can be different from the calculated band gap due to some causes such as the exciton binding energy and Stokes effect.[49,50] Despite these drawbacks, the DFT results are known to be accurate enough to predict the physical mechanism and show a reliable trend in the band gap by a certain effect.[46] In monolayer Sc_2CO_2, there is a possibility that the recombination of the excited electron–hole pairs can occur from the K or Γ point in the lowest conduction band.

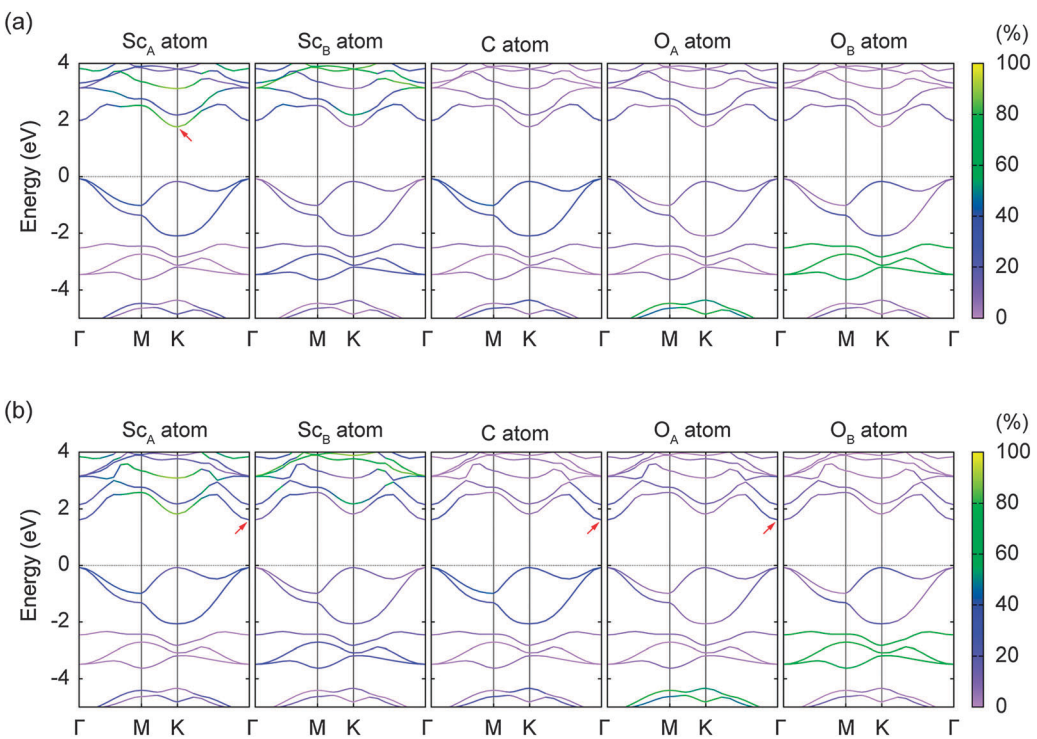

Fig. 4 Contribution of each atom in monolayer Sc_2CO_2 to the energy level under the (a) E-field-free state and (b) positive E-field of 5 V nm^{-1}, respectively. Percentages of the contributions of each atom are marked in a different color. The red arrows represent the CBM state at the band structure of the dominant atoms.

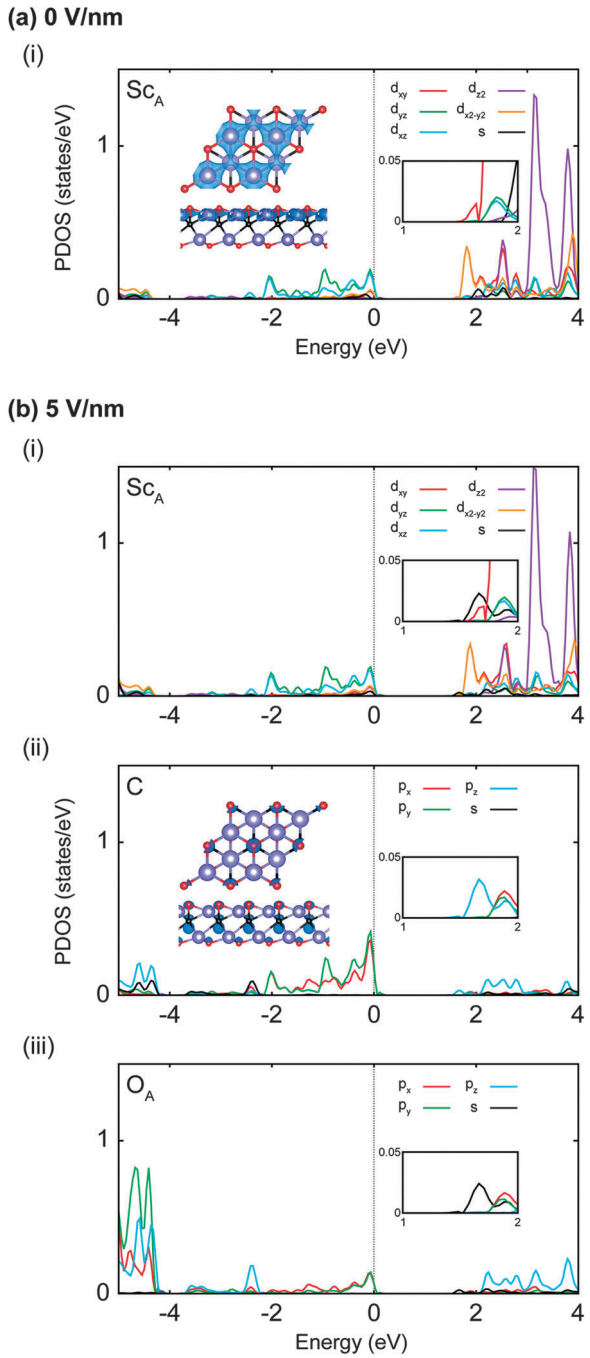

Fig. 5 PDOS of the major atoms under an external E-field of 0 and 5 V nm^{-1}. (a) PDOS of the Sc_A atom under the E-field-free state, and (b) (i)–(iii) PDOS of the Sc_A, C, and O_A atoms under 5 V nm^{-1}, respectively. Each orbital is represented by the differently colored lines. The insets in (a) and (b-ii) represent the energy distribution at the CBM state under the E-field of 0 and 5 V nm^{-1}, respectively.

For this reason, effective masses at the K and Γ points in the lowest conduction band were calculated to confirm a recombination pathway. Here, the effective mass was decided by an inversely proportional value to the curvature of the band structure. From the calculation, while the effective mass in the K point is originally 6% heavier than that in the Γ point with no electric field, the effective mass in the Γ point becomes 4% greater than that in the K point in the lowest conduction band under 5 V nm^{-1}. This difference means that each lower point in the lowest conduction band at 0 and 5 V nm^{-1} has a heavier exciton and larger exciton binding energy.[50,51] From this consideration, the K to Γ indirect and Γ to Γ direct recombination are favored in monolayer Sc_2CO_2 under 0 and 5 V nm^{-1}, respectively. Thus, the present findings that the indirect to direct band gap transition occurs by an external E-field in the monolayer Sc_2CO_2 system can be undoubtedly supported. However, to obtain the exact value of the band gap in this system, more studies need to be discussed further with other functionals like the B3PW91.[52]

Conclusion

In summary, DFT calculations were performed to investigate the change of the band gap properties in an oxygen functionalized-monolayer Sc_2C system by a perpendicular external E-field. The band gap size of monolayer Sc_2CO_2 has a linear increment with a small slope as the external E-field varies from −5 to 3.7 V nm^{-1}. However, there is an indirect to direct band gap transition at about 3.7 V nm^{-1}, and the band gap size is rapidly decreased after the band gap transition. The great variations *via* the E-field in monolayer Sc_2CO_2 are unique phenomena in single-layer systems. In monolayer Sc_2CO_2, the band gap transition is exhibited because the Γ point in the lowest conduction band responds more sensitively to the perpendicular external E-field than the K point, which is the original CBM state. The difference in response of each point to the perpendicular E-field originates from the fact that the in-plane orbitals mainly contribute to the K point in the lowest conduction band, whereas the Γ point is comprised of the out-of-plane orbitals. The present work opens the opportunity for monolayer MXene to become a promising material in opto-electronics and optics.

Acknowledgements

This research was supported by the Basic Science Research Program through the National Research Foundation of Korea (NRF) funded by the Ministry of Education (2013R1A1A2A10064432).

References

1 J. Ortega, M. Aguilar-Frutis, G. Alarcón, C. Falcony, V. Méndez-Garcia and J. Araiza, *Mater. Sci. Eng., B*, 2014, **187**, 83–88.
2 L. Lin, Z. Li, J. Feng and Z. Zhang, *Phys. Chem. Chem. Phys.*, 2013, **15**, 6063–6067.
3 Q. Chen, H. Hu, X. Chen and J. Wang, *Appl. Phys. Lett.*, 2011, **98**, 053102.
4 J. K. Ellis, M. J. Lucero and G. E. Scuseria, *Appl. Phys. Lett.*, 2011, **99**, 261908.
5 A. Kuc, N. Zibouche and T. Heine, *Phys. Rev. B: Condens. Matter Mater. Phys.*, 2011, **83**, 245213.

6 W. S. Yun, S. Han, S. C. Hong, I. G. Kim and J. Lee, *Phys. Rev. B: Condens. Matter Mater. Phys.*, 2012, **85**, 033305.
7 H. Shi, H. Pan, Y.-W. Zhang and B. I. Yakobson, *Phys. Rev. B: Condens. Matter Mater. Phys.*, 2013, **87**, 155304.
8 Z. Zhang, M. Si, Y. Wang, X. Gao, D. Sung, S. Hong and J. He, *J. Chem. Phys.*, 2014, **140**, 174707.
9 P. Moontragoon, Z. Ikonić and P. Harrison, *Semicond. Sci. Technol.*, 2007, **22**, 742.
10 L. Shi, Y. Qin, J. Hu, Y. Duan, L. Qu, L. Wu and G. Tang, *Europhys. Lett.*, 2014, **106**, 57001.
11 M. Naguib, M. Kurtoglu, V. Presser, J. Lu, J. Niu, M. Heon, L. Hultman, Y. Gogotsi and M. W. Barsoum, *Adv. Mater.*, 2011, **23**, 4248–4253.
12 M. Naguib, O. Mashtalir, J. Carle, V. Presser, J. Lu, L. Hultman, Y. Gogotsi and M. W. Barsoum, *ACS Nano*, 2012, **6**, 1322–1331.
13 M. Naguib, J. Halim, J. Lu, K. M. Cook, L. Hultman, Y. Gogotsi and M. W. Barsoum, *J. Am. Chem. Soc.*, 2013, **135**, 15966–15969.
14 O. Mashtalir, M. Naguib, B. Dyatkin, Y. Gogotsi and M. W. Barsoum, *Mater. Chem. Phys.*, 2013, **139**, 147–152.
15 A. L. Ivanovskii and A. N. Enyashin, *Russ. Chem. Rev.*, 2013, **82**, 735–746.
16 M. Naguib, V. N. Mochalin, M. W. Barsoum and Y. Gogotsi, *Adv. Mater.*, 2014, **26**, 992–1005.
17 M. Khazaei, M. Arai, T. Sasaki, C.-Y. Chung, N. S. Venkataramanan, M. Estili, Y. Sakka and Y. Kawazoe, *Adv. Funct. Mater.*, 2013, **23**, 2185–2192.
18 M. Khazaei, M. Arai, T. Sasaki, M. Estili and Y. Sakka, *Phys. Chem. Chem. Phys.*, 2014, **16**, 7841–7849.
19 E. V. Castro, K. Novoselov, S. Morozov, N. Peres, J. L. Dos Santos, J. Nilsson, F. Guinea, A. Geim and A. C. Neto, *Phys. Rev. Lett.*, 2007, **99**, 216802.
20 D. K. Samarakoon and X.-Q. Wang, *ACS Nano*, 2010, **4**, 4126–4130.
21 A. Ramasubramaniam, D. Naveh and E. Towe, *Nano Lett.*, 2011, **11**, 1070–1075.
22 A. Ramasubramaniam, D. Naveh and E. Towe, *Phys. Rev. B: Condens. Matter Mater. Phys.*, 2011, **84**, 205325.
23 R. Quhe, J. Zheng, G. Luo, Q. Liu, R. Qin, J. Zhou, D. Yu, S. Nagase, W.-N. Mei, Z. Gao and J. Lu, *NPG Asia Mater.*, 2012, **4**, e6.
24 D. Xu, H. He, R. Pandey and S. P. Karna, *J. Phys.: Condens. Matter*, 2013, **25**, 345302.
25 Z. Ni, Q. Liu, K. Tang, J. Zheng, J. Zhou, R. Qin, Z. Gao, D. Yu and J. Lu, *Nano Lett.*, 2011, **12**, 113–118.
26 N. Drummond, V. Zolyomi and V. Fal'Ko, *Phys. Rev. B: Condens. Matter Mater. Phys.*, 2012, **85**, 075423.
27 B. Mohan, A. Kumar and P. Ahluwalia, *Physica E*, 2012, **44**, 1670–1674.
28 A. Bouhemadou, R. Khenata, M. Kharoubi and Y. Medkour, *Solid State Commun.*, 2008, **146**, 175–180.
29 Q. Tang, Z. Zhou and P. Shen, *J. Am. Chem. Soc.*, 2012, **134**, 16909–16916.
30 L.-Y. Gan, Y.-J. Zhao, D. Huang and U. Schwingenschlögl, *Phys. Rev. B: Condens. Matter Mater. Phys.*, 2013, **87**, 245307.
31 Q. Hu, D. Sun, Q. Wu, H. Wang, L. Wang, B. Liu, A. Zhou and J. He, *J. Phys. Chem. A*, 2013, **117**, 14253–14260.
32 Q. Peng, J. Guo, Q. Zhang, J. Xiang, B. Liu, A. Zhou, R. Liu and Y. Tian, *J. Am. Chem. Soc.*, 2014, **136**, 4113–4116.
33 Y. Xie, M. Naguib, V. N. Mochalin, M. W. Barsoum, Y. Gogotsi, X. Yu, K.-W. Nam, X.-Q. Yang, A. I. Kolesnikov and P. R. Kent, *J. Am. Chem. Soc.*, 2014, **136**, 6385–6394.
34 J. Halim, M. R. Lukatskaya, K. M. Cook, J. Lu, C. R. Smith, L.-Å. Naslund, S. J. May, L. Hultman, Y. Gogotsi, P. Eklund and M. W. Barsoum, *Chem. Mater.*, 2014, **26**, 2374–2381.
35 Z. Ma, Z. Hu, X. Zhao, Q. Tang, D. Wu, Z. Zhou and L. Zhang, *J. Phys. Chem. C*, 2014, **118**, 5593–5599.
36 Q. Hu, H. Wang, Q. Wu, X. Ye, A. Zhou, D. Sun, L. Wang, B. Liu and J. He, *Int. J. Hydrogen Energy*, 2014, **39**, 10606–10612.
37 Y. Gao, L. Wang, Z. Li, A. Zhou, Q. Hu and X. Cao, *Solid State Sci.*, 2014, **35**, 62–65.
38 D. Er, J. Li, M. Naguib, Y. Gogotsi and V. B. Shenoy, *ACS Appl. Mater. Interfaces*, 2014, **6**, 11173–11179.
39 G. Kresse and J. Hafner, *Phys. Rev. B: Condens. Matter Mater. Phys.*, 1993, **47**, 558.
40 G. Kresse and J. Furthmüller, *Comput. Mater. Sci.*, 1996, **6**, 15–50.
41 G. Kresse and J. Furthmüller, *Phys. Rev. B: Condens. Matter Mater. Phys.*, 1996, **54**, 11169.
42 J. P. Perdew, K. Burke and M. Ernzerhof, *Phys. Rev. Lett.*, 1996, **77**, 3865.
43 G. Kresse and D. Joubert, *Phys. Rev. B: Condens. Matter Mater. Phys.*, 1999, **59**, 1758.
44 H. J. Monkhorst and J. D. Pack, *Phys. Rev. B: Solid State*, 1976, **13**, 5188–5192.
45 J. Neugebauer and M. Scheffler, *Phys. Rev. B: Condens. Matter Mater. Phys.*, 1992, **46**, 16067.
46 L. Kou, T. Frauenheim and C. Chen, *J. Phys. Chem. Lett.*, 2013, **4**, 1730–1736.
47 S. Horzum, H. Sahin, S. Cahangirov, P. Cudazzo, A. Rubio, T. Serin and F. Peeters, *Phys. Rev. B: Condens. Matter Mater. Phys.*, 2013, **87**, 125415.
48 Y.-S. Kim, M. Marsman, G. Kresse, F. Tran and P. Blaha, *Phys. Rev. B: Condens. Matter Mater. Phys.*, 2010, **82**, 205212.
49 J.-L. Bredas, *Mater. Horiz.*, 2014, **1**, 17–19.
50 W. Zhao, R. M. Ribeiro, M. Toh, A. Carvalho, C. Kloc, A. Castro Neto and G. Eda, *Nano Lett.*, 2013, **13**, 5627–5634.
51 M. Dvorak, S.-H. Wei and Z. Wu, *Phys. Rev. Lett.*, 2013, **110**, 016402.
52 H. Xiao, J. Tahir-Kheli and W. A. Goddard III, *J. Phys. Chem. Lett.*, 2011, **2**, 212–217.

